The Astrophysical Journal Letters, 709:L21–L25, 2010 January 20 doi:10.1088/2041-8205/709/1/L21

STRUCTURE AND MORPHOLOGIES OF $z \sim 7$–8 GALAXIES FROM ULTRA-DEEP WFC3/IR IMAGING OF THE HUBBLE ULTRA-DEEP FIELD*

P. A. Oesch[1], R. J. Bouwens[2], C. M. Carollo[1], G. D. Illingworth[2], M. Trenti[3], M. Stiavelli[4], D. Magee[2], I. Labbé[5,7], and M. Franx[6]
[1] Institute for Astronomy, ETH Zurich, 8092 Zurich, Switzerland; poesch@phys.ethz.ch
[2] UCO/Lick Observatory, University of California, Santa Cruz, CA 95064, USA
[3] Center for Astrophysics and Space Astronomy, University of Colorado, 389-UCB, Boulder, CO 80309, USA
[4] Space Telescope Science Institute, Baltimore, MD 21218, USA
[5] Carnegie Observatories, Pasadena, CA 91101, USA
[6] Leiden Observatory, Leiden University, NL-2300 RA Leiden, The Netherlands
Received 2009 September 29; accepted 2009 December 8; published 2009 December 29

ABSTRACT

We present a first morphological study of $z \sim 7$–8 Lyman break galaxies (LBGs) from Oesch et al. and Bouwens et al. detected in ultra-deep near-infrared imaging of the Hubble Ultra-Deep Field (HUDF) by the HUDF09 program. With an average intrinsic size of 0.7 ± 0.3 kpc, these galaxies are found to be extremely compact, having an average observed surface brightness of $\mu_J \simeq 26$ mag arcsec^{-2}, and only two out of the full sample of 16 $z \sim 7$ galaxies show extended features with resolved double cores. By comparison to lower redshift LBGs, it is found that only little size evolution takes place from $z \sim 7$ to $z \sim 6$, while galaxies between $z \sim 4$–5 show more extended wings in their apparent profiles. The average size scales as $(1+z)^{-m}$ with $m = 1.12 \pm 0.17$ for galaxies with luminosities in the range $(0.3\text{–}1)L^*_{z=3}$ and with $m = 1.32 \pm 0.52$ for $(0.12\text{–}0.3)L^*_{z=3}$, consistent with galaxies having constant comoving sizes. The peak of the size distribution changes only slowly from $z \sim 7$ to $z \sim 4$. However, a tail of larger galaxies ($\gtrsim$1.2 kpc) is gradually built up toward later cosmic times, possibly via hierarchical build-up or via enhanced accretion of cold gas. Additionally, the average star formation surface density of LBGs with luminosities $(0.3\text{–}1)L^*_{z=3}$ is nearly constant at $\Sigma_{\rm SFR} = 1.9\ M_\odot\ {\rm yr}^{-1}\ {\rm kpc}^{-2}$ over the entire redshift range $z \sim 4$–7 suggesting similar star formation efficiencies at these early epochs. The above evolutionary trends seem to hold out to $z \sim 8$ though the sample is still small and possibly incomplete.

Key words: galaxies: evolution – galaxies: high-redshift – galaxies: structure

1. INTRODUCTION

The newly installed WFC3/IR camera on the *Hubble Space Telescope* (*HST*) has opened up a new territory in the study of galaxies at $z \gtrsim 6.5$. Its increased capability has led to numerous detections of galaxies at $z \gtrsim 6.5$ already in the first epoch data of the HUDF09 (Oesch et al. 2010; Bouwens et al. 2009a; McLure et al. 2009; Bunker et al. 2009).

Understanding the evolution of galaxy sizes and morphologies out to $z \gtrsim 6.5$ can provide essential clues to galaxy formation models. While hydrodynamical galaxy formation simulations of Lyman break galaxies (LBGs; e.g., Finlator et al. 2006; Night et al. 2006; Nagamine et al. 2008) have focused on the prediction of the evolution of the galaxy luminosity and mass functions, the sizes of these galaxies have not been addressed in great detail so far. By providing these results we hope to stimulate interest in this key aspect of galaxies at early times.

Based on semianalytical modeling, the sizes of LBGs at fixed luminosity are expected to slowly decrease toward earlier cosmic times (Mo et al. 1998, 1999), which is in good agreement with earlier observations of LBGs (e.g., Ferguson et al. 2004; Bouwens et al. 2004).

The UV morphologies of LBGs have been studied between $z \sim 2$–6 from both ground-based and *HST* imaging. They have been found to be very compact, but often containing multiple cores, especially at brighter magnitudes (e.g., Giavalisco et al. 1996; Lowenthal et al. 1997; Ravindranath et al. 2006; Lotz et al. 2006; Law et al. 2007; Conselice & Arnold 2009). The dominant mechanism for star formation in these galaxies is still debated. LBGs with multiple cores have been interpreted as merging systems, with star formation triggered by this interaction, which is a natural scenario in a hierarchical universe (e.g., Somerville et al. 2001; Overzier et al. 2008). However, these individual cores could also originate from individual star-forming clumps within a larger gas-dominated disk galaxy, whereby this clumpy state is kept alive due to gas streams replenishing the disk galaxy with cold gas (e.g., Dekel et al. 2009).

Here, we present the highest resolution observations available to date of galaxies from a time when the universe was only ~800 Myr old. Our analysis is primarily based on the sample of 16 $z \sim 7$ LBGs from Oesch et al. (2010). We also discuss the 5 $z \sim 8$ objects identified by Bouwens et al. (2009a). These galaxies are detected in the first epoch ultra-deep WFC3/IR imaging of the HUDF09 survey, which reaches ~29 mag (5σ) in $Y_{105}J_{125}H_{160}$photometry over an area of 4.7 arcmin^2 covering the Hubble Ultra-Deep Field (HUDF; Beckwith et al. 2006). The 16 $z \sim 7$ galaxy candidates are selected based on their $(z_{850} - Y_{105})$ versus $(Y_{105} - J_{125})$ colors using the Lyman Break Technique (e.g., Steidel et al. 1996) and have an expected redshift distribution $z \sim 6.5$–7.5 with a median at $\langle z \rangle = 6.8$. Similarly, the $z \sim 8$ sample is selected based on their $(Y_{105} - J_{125})$ versus $(J_{125} - H_{160})$ colors. For more information on the survey and the galaxy sample, we refer to Oesch et al. (2010) and Bouwens et al. (2009a). We also include galaxies from $z \sim 4$–6 identified as dropout galaxies in the optical HUDF data for comparison with the $z \gtrsim 6.5$ population.

* Based on data obtained with the *Hubble Space Telescope* operated by AURA, Inc. for NASA under contract NAS5-26555.
[7] Hubble Fellow.

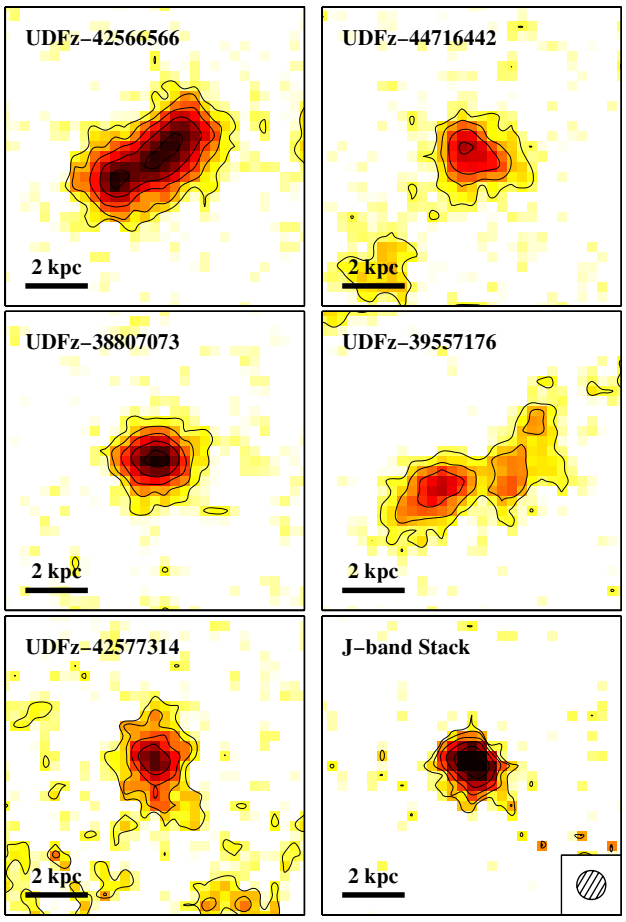

Figure 1. Surface brightness contours of the five brightest galaxies in our sample and of a J_{125} stack of the remaining 11 fainter galaxies (last panel in lower right). The first five images are superpositions of Y_{105}, J_{125}, and H_{160} exposures, with the contour lines corresponding to $\mu_{\rm YJH} = 23.5$–25.5 mag arcsec^{-2} in steps of 0.5 mag arcsec^{-2}. The bar in the left corner indicates 2 kpc (physical) at $z = 6.8$ the expected mean redshift of these galaxies. All images are 1.″8 on a side. The size (FWHM) of the J_{125} PSF is shown as an inset in the lower right panel for comparison.

We adopt $\Omega_M = 0.3, \Omega_\Lambda = 0.7, H_0 = 70$ km s^{-1} Mpc^{-1}, i.e., $h = 0.7$. Magnitudes are given in the AB system (Oke & Gunn 1983). We express galaxy UV luminosities in units of the characteristic luminosity at $z \sim 3$ being $M_{1600}(z = 3) = -21.0$ (Steidel et al. 1999).

2. MORPHOLOGIES AT $z \sim 7$

The $z \sim 7$ galaxies are extremely compact as can be seen from the contour plots in Figure 1, where we show the individual summed Y_{105}, J_{125}, and H_{160} observations of the five brightest sources and additionally a J_{125} stack of the remaining 11 fainter ones (for stamps of individual sources, see Oesch et al. 2010). As can be seen, the average $z \sim 7$ galaxy appears to be very symmetric and compact; with two exceptions, no extended features can be identified. The two exceptions are as follows.

1. The galaxy UDFz-42566566 is the brightest galaxy in our sample and consists of two clearly distinct components, separated by 2 kpc. These two each contribute about the same amount of light (1:1.2) with very similar colors. They have individual half-light radii of 0.5 kpc and 0.8 kpc, respectively, very similar to the compact galaxies in our sample. One interpretation for the origin of the individual components is therefore that they are in a merging phase. The linear geometry of the whole galaxy, however, may also suggest that the individual clumps are star-forming regions within a disk structure, similar to what has been found at $z \sim 2$ in observations and simulations.
2. The galaxy UDFz-39557176 also consists of at least two components. The total light of this galaxy is dominated by a slightly elongated central structure, which has a fainter counterpart about 2 kpc away to the NW. The flux ratio of these two is 1:1.4. It is worth noting that this galaxy has been split into two sources in the McLure et al. (2009) catalog. However, the two knots are most probably physically connected and are about to merge with each other. The fainter component to the NW shows a significantly redder $Y_{105} - J_{125}$ color compared to the central core by 0.2 mag, and also a redder $J_{125} - H_{160}$ color by 0.1 mag. This may indicate that the second component consists of older stellar populations. However, a more speculative explanation could be that the second component is reddened due to dust from the central core. This would imply that these galaxies contain a more extended gas disk than what can be seen from their UV light.

3. COMPARISON TO LBGs AT $z \sim 4$–6

In order to quantify the evolution of galaxy structures across cosmic time, we compare the $z \sim 7$ galaxies with LBGs identified at $z \sim 4$–6. We focus on three main aspects: (1) the size evolution, (2) the evolution of the average galaxy light profile, and (3) the evolution of the surface density of star formation in these galaxies.

3.1. Size Evolution

Galaxy sizes are measured using circular apertures containing 50% of the galaxies' light. We use the observed half-light radius from SExtractor, $r^{\rm obs}_{1/2,\rm SE}$, and correct it for the point-spread function (PSF) broadening according to $r_{1/2,\rm SE} = \sqrt{(r^{\rm obs}_{1/2,\rm SE})^2 - r^2_{\rm PSF}}$. The radius $r_{\rm PSF}$ of a point source is 0.″12 in the J_{125}, and 0.″11 in the Y_{105} observations. These measurements are checked against the higher resolution optical data for the $z \sim 5$ population where size measurement from both Advanced Camera for Surveys (ACS; i_{775}) and WFC3/IR (Y_{105}) is available. No significant differences are found, showing the robustness of these size estimates even for such faint, small galaxies and the validity of the simple PSF correction.

As a second check, we adopt size measurements based on `galfit` (Peng et al. 2002). Single sersic profiles are fitted to these galaxies with sersic indices fixed at $n = 1.5$, the value measured for a mean stack of $z \sim 4$ LBGs. The half-light radii estimates of the best-fit models are in good agreement with the SExtractor measurements with a dispersion of $\sigma_r = 0.''05$ and no bias. Similar results are found when using an average Sersic index $n = 1$, or $n = 3$. However, `galfit` fails to return reliable measurements when the light profile is not well approximated by a single-component fit and we use the SExtractor measurements as our fiducial ones. When appropriate, we also comment on the implications of using the `galfit` measurements.

Due to selection effects, large, low-surface brightness galaxies will be missed in our catalog. We estimate this bias by inserting artificial galaxies of fixed profiles into the science images and rerunning the detection algorithm with the same parameters as for the creation of the original catalogs (for more details, see Oesch et al. 2007). The galaxy profiles are chosen to follow an

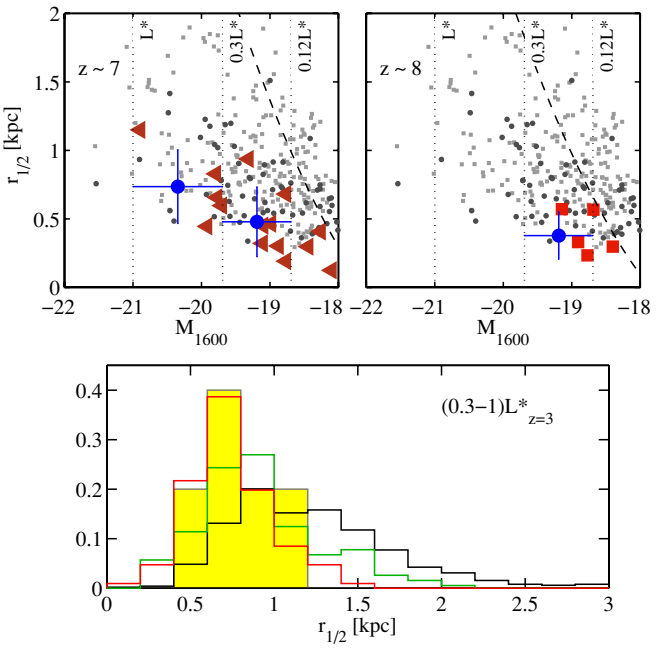

Figure 2. Top: luminosity-size relation for $z \sim 5$–8 galaxies in the WFC3/IR observations. The colored points are the $z \sim 7$ (left) and $z \sim 8$ galaxies (right). Dark gray dots represent samples of $z \sim 5$–6 based on WFC3/IR observations, while light gray squares are $z \sim 4$ galaxies based on optical ACS data for comparison. All sizes are PSF corrected. The dashed line indicates the 50% completeness for galaxies with exponential profiles shifted to the absolute magnitude at the given redshift. The vertical dotted lines correspond to the edges of the luminosity bins with 0.12, 0.3, $1L^*_{z=3}$. The blue points mark the mean of the $z \sim 7$ population in the given luminosity bin. Bottom: comparison of the size distribution of $z \sim 4$–7 galaxies in the luminosity range $(0.3–1)L^*_{z=3}$. The filled yellow histogram is for $z \sim 7$ galaxies, the others are for lower redshift LBGs (red: $z \sim 6$, green: $z \sim 5$, black: $z \sim 4$). In order to increase statistics, this plot is based on GOODS for the galaxies of $z \sim 4$–6, where the sizes are measured from SExtractor in the i_{775} ($z \sim 4$) and z_{850}($z \sim 5$–6). The $z \sim 7$ measurements are based on the J_{125}. The main difference is the tail toward larger sizes at later cosmic times, while the peak of the size distribution changes little.

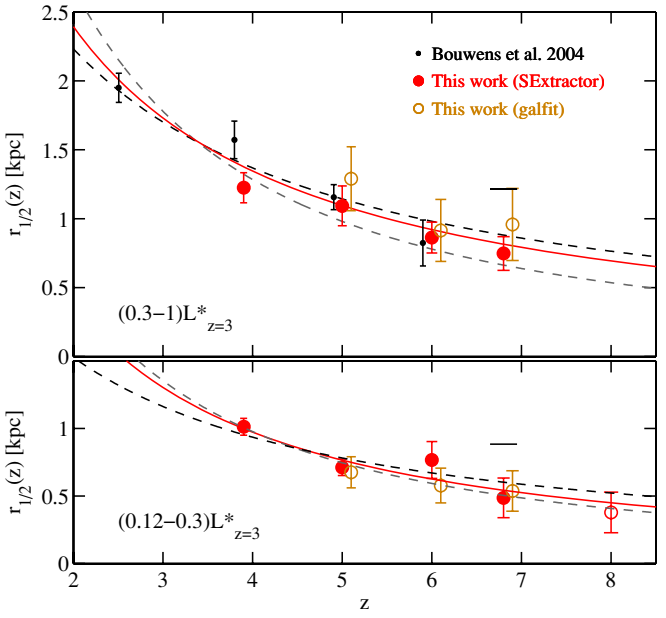

Figure 3. Evolution of the mean galaxy size across the redshift range $z \sim 2$–8 in two different luminosity ranges $(0.3–1)L^*_{z=3}$ (top) and $(0.12–0.3)L^*_{z=3}$ (bottom). The data from this work are plotted as red dots and are based on the PSF corrected SExtractor half-light radii. Also reported are the measurements from Bouwens et al. (2004) based on optical ACS data of the same luminosity range. These points are repeated in the lower panel for comparison. Mean half-light radius measurements from Sersic fits with galfit are shown as orange circles, offset from their redshift by 0.1. The dashed lines indicate the scaling expected for a fixed halo mass ($\propto H(z)^{-2/3}$; black) and at fixed halo circular velocity ($\propto H(z)^{-1}$; gray). The red lines correspond to the best fit to the observed evolution described by $(1+z)^{-m}$, with $m = 1.12 \pm 0.17$ for the brighter luminosity bin, and $m = 1.32 \pm 0.52$ at fainter luminosities. These are formally identical and are consistent with the $m \sim 1$ value derived previously. The short black line at $z \sim 7$ indicates the mean sizes found when projecting the observed $z \sim 4$ sample to $z \sim 7$, while keeping their luminosities and physical sizes constant in order to test for measurement biases due to cosmological surface brightness dimming.

exponential Sersic function ($n = 1$) and a de Vaucouleur profile ($n = 4$).

In the upper panel of Figure 2, we plot the half-light radii against the absolute magnitudes for the $z \sim 7$–8 galaxies and both $z \sim 5$–6 and $z \sim 4$ samples. As can be seen, the $z \sim 7$ sample is complete for all galaxies at 1 kpc down to $M_{1600} = -18.7$, corresponding to $0.12L^*_{z=3}$. At these same luminosities the galaxies in the $z \sim 8$ sample are close to the completeness limit. We therefore do not include the $z \sim 8$ sample when fitting scaling relations as a function of redshift in our analysis.

As can be seen from the figure, at fixed luminosities, the sizes evolve only little from $z \sim 4$–8. However, the lower redshift population contains an extended tail toward galaxies with sizes $\gtrsim$1.2 kpc, which is not seen at higher redshifts as shown in the lower panel of Figure 2. In order to increase the statistics, the $z \sim 4$–6 galaxy samples are taken from GOODS based on ACS imaging (e.g., Giavalisco et al. 2004a, 2004b). The peaks of the distributions are between 0.8 and 1 kpc for all redshifts. The $z \sim 4$ population contains a significant population of galaxies with $\gtrsim$1.2 kpc, which are completely absent at $z \sim 7$. Firm confirmation of the lack of such large objects at $z \sim 7$ will require larger area surveys, but the trend seen from $z \sim 6$ to lower redshift is very suggestive. It indicates a scenario in which these primordial star-forming galaxies are formed as small clumps with a size of ~0.4–0.8 kpc independent of luminosity. Toward later cosmic times, hierarchical build-up or enhanced accretion of cold gas starts to produce a tail of larger galaxies, but changing the peak only little.

The evolution of the average sizes of galaxies from $z \sim 2$–8 is plotted in Figure 3 for two different luminosity ranges, $(0.3–1)L^*_{z=3}$ (top) and $(0.12–0.3)L^*_{z=3}$ (bottom). The expected size scaling from semianalytical models is $H(z)^{-1}$, at fixed halo circular velocity, or $H(z)^{-2/3}$ at fixed halo mass (Mo et al. 1998), where $H(z)$ is the Hubble parameter at redshift z which scales as $\sim(1+z)^{3/2}$ at $z > 2$. The observed size evolution at fixed luminosity is fitted with a scaling of the form $(1+z)^{-m}$. The two fits are formally identical with $m = 1.12 \pm 0.17$ and $m = 1.32 \pm 0.52$, respectively. This is in agreement with previous estimates where the sizes were found to scale roughly according to $(1+z)^{-1}$ (Bouwens et al. 2004, 2006). However, $H(z)^{-1}$ (Ferguson et al. 2004; Hathi et al. 2008b) cannot be ruled out as both scalings are very flat over our redshift range and diverge only at lower z.

Note that the observed evolution in sizes is not an artifact of cosmological surface brightness dimming. We verified this by artificially redshifting our $z \sim 4$ sample (i_{775} band) to $z \sim 7$ (J_{125} band) and remeasuring their sizes with SExtractor. For the more luminous galaxies, the input size is recovered perfectly, while for the lower luminosity sample only a small bias of ~10% toward smaller sizes is found due to the flux loss in the galaxy wings.

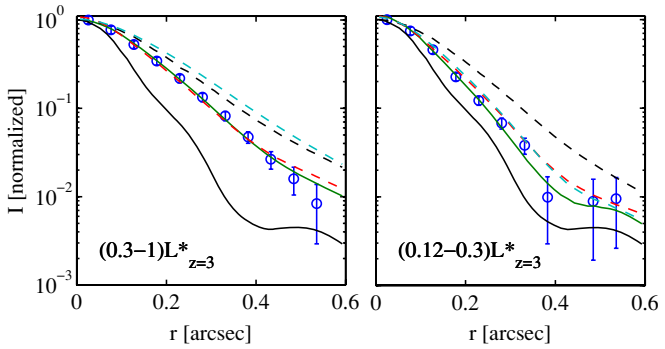

Figure 4. Apparent intensity profiles of the stacked $z \sim 4$–7 galaxies in two different luminosity ranges, $(0.3–1)L^*_{z=3}$ (left) and $(0.12–0.3)L^*_{z=3}$ (right). The blue points are the data, while the black line is the PSF from stars in the J_{125} observation. The best-fit model of the $z \sim 7$ population is shown as a solid green line. Models for lower redshift galaxies are shown as dashed lines in red ($z \sim 6$), cyan ($z \sim 5$), and black ($z \sim 4$). For galaxies with luminosities $(0.3–1)L^*_{z=3}$, the $z \sim 4$–5 population shows clearly extended wings with respect to higher redshift galaxies, while in the lower luminosity bin, the evolution is slower. Note that this is consistent with increasing physical sizes toward lower redshifts due to increasing angular diameter distances.

3.2. Average Profiles

In order to test the uniformity of average galaxy sizes over these redshifts, we measure their average profiles based on stacking galaxies from fixed luminosity ranges and fitting these profiles with `galfit`. For the $z \sim 7$ galaxies this is done in the J_{125} band, corresponding closely to rest frame 1600 Å. The galaxy stamps are cleaned of close neighbors using the cleaning algorithm of `ZEST+` (C. M. Carollo et al. 2010, in preparation). The algorithm masks neighboring sources in the images and replaces contaminated pixels with background noise. The PSF was estimated on three stars which showed no saturation in individual exposures. We have also ensured that the central pixels of the stars have not been affected by cosmic-ray rejection in the data reduction pipeline.

The above procedure is repeated in the Y_{105} band for samples of $z \sim 5$ and $z \sim 6$ galaxies, extracted from the optical HUDF catalogs. The Y_{105} corresponds to 1750 Å and 1500 Å rest frame at $z \sim 5$ and $z \sim 6$ respectively. For the $z \sim 4$ population, the i_{775} band corresponds most closely to the 1600 Å wavelength. Therefore morphological k-correction effects are minimal.

A Sersic profile is fitted to these stacked images from all three redshift bins and both luminosity ranges. Through simulations, we have verified that the stacking procedure reproduces the average profiles of a galaxy population accurately (see also Hathi et al. 2008a). In order to compare the different profiles directly, we have convolved the best-fit models with the J_{125} band PSF and show the result in Figure 4. The faint $z \sim 7$ galaxies are only marginally resolved. The average profile is remarkably similar at all redshifts from $z \sim 4$ to $z \sim 7$, except for the appearance of extended wings at $z \sim 4$ for all luminosities, and extended wings at $z \sim 5$ for the more luminous galaxies. But even the similar angular size indicates increasing physical sizes toward lower redshifts due to increasing angular diameter distances (30% larger at $z \sim 4$ versus $z \sim 7$).

The steepness of all these profiles suggests that star formation is largely centrally concentrated in these galaxies and not widely distributed in a large, clumpy disk.

3.3. SFR Surface Density

Given the slow evolution of the sizes of LBGs, it is interesting to estimate the change in the average surface density of star formation, $\Sigma_{\rm SFR}$. The upper panel of Figure 5 shows this as a function of absolute magnitude. The star formation rate (SFR) has been estimated based on a simple conversion of the UV luminosity to SFR (Madau et al. 1998) assuming a Salpeter initial-mass function. For the $z \sim 7$ galaxies the SFRs range from $\sim$1 to $10 M_\odot$ yr^{-1}. Furthermore, our results suggest that the average $\Sigma_{\rm SFR}$ remains relatively constant for the whole redshift range from $z \sim 7$ to $z \sim 4$. This is shown for galaxies with luminosities in the range $(0.3–1)L^*_{z=3}$ in the lower panel of Figure 5. Filled red circles represent the actual measured values, while the orange open circles are corrected for dust extinction using the formula by Meurer et al. (1999) and UV continuum slopes measured in this same luminosity and redshift ranges from Bouwens et al. (2009b). In agreement with the size evolution, there is a small trend toward lower apparent $\Sigma_{\rm SFR}$ at lower redshifts. However, when corrected for dust extinction, the star formation surface density is consistent with being constant over the entire redshift range $z \sim 3$–7.

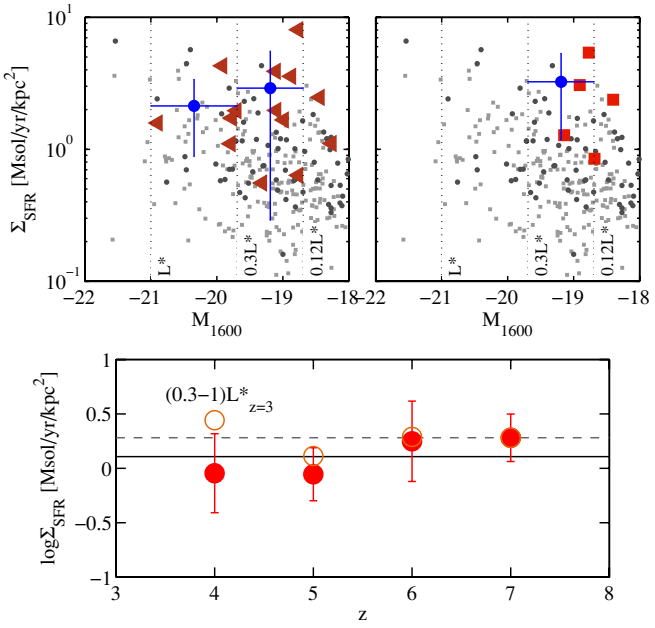

Figure 5. Top: Surface density of star formation against luminosity. As in Figure 2, the gray background points represent the $z \sim 4$–6 population in the WFC3/IR data and the colored points are the $z \sim 7$ (left) and 8 population (right). Bottom: the mean surface density of the SFR against redshift. Red dots correspond to the actual measurements, while the orange circles are corrected for dust absorption (Bouwens et al. 2009b). The black line is the average for the uncorrected values and the dashed line is the same for the dust corrected ones. In both cases, the average $\Sigma_{\rm SFR}$ is consistent with being constant over the entire redshift range $z \sim 4$–7.

A possible explanation for the constancy of the star formation surface density is that the average star formation efficiency is very similar in all these galaxies and that feedback effects change the mode of star formation only little in these primordial galaxies. Note that this result is consistent with a constant limiting surface brightness from $z \sim 7$ down to local galaxies (see Meurer et al. 1997; Hathi et al. 2008b). However, there are exceptions from this typical mode of star formation. For example, the average surface density of star formation is almost 3 orders of magnitudes larger in hyper-starbursts in quasar hosts at similar redshifts ($z = 6.42$; Walter et al. 2009).

4. SUMMARY AND CONCLUSIONS

We have used the ultra-deep WFC3/IR observations of the HUDF09 program to study the structures and morphologies of

$z \gtrsim 6.5$ galaxies previously presented in Oesch et al. (2010) and Bouwens et al. (2009a). These galaxies are all extremely compact, with an average size of 0.7 ± 0.3 kpc. Only two out of the 16 $z \sim 7$ galaxies show a double core. This fraction is slightly smaller than the ∼30% of LBGs with disturbed morphologies and double cores found at lower redshifts (e.g., Lotz et al. 2006; Conselice & Arnold 2009; Petty et al. 2009), although they are still consistent within the small number statistics. The $z \sim 7$ galaxies are extremely similar to the $z \sim 6$ population, both in sizes and in their average light profiles, showing that galaxy evolution proceeds slowly over the ∼170 Myr from $z \sim 7$–6.

By comparison to LBGs down to $z \sim 4$ only a very slow size evolution is found, following $(1+z)^{-m}$, with $m = 1.12 \pm 0.17$ for galaxies of luminosities $(0.3–1)L^*_{z=3}$. Fainter galaxies down to $0.12L^*_{z=3}$ follow a similar scaling with $m = 1.32 \pm 0.52$. Additionally, the mean star formation surface densities of LBGs are found to be constant over the entire redshift range $z \sim 4$–7, which may be explained by largely constant star formation efficiencies at these early epochs.

Similar exponents for the size scalings with redshift have been found for disk galaxies between $z \sim 0$–3 (e.g., Buitrago et al. 2008), as well as from semianalytical modeling including concentrated dark-matter halo profiles (e.g., Somerville et al. 2008; Firmani et al. 2009)

By extending the present study to larger samples of $z \sim 7$ galaxies which will become available in the near future, it will be possible to put more stringent constraints on galaxy evolution models and to shed more light on the question of the main driver of star formation in LBGs at these early epochs.

We especially thank all those at NASA, STScI, and throughout the community who have worked so diligently to make *Hubble* the remarkable observatory that it is today. The servicing missions have rejuvenated *HST* and made it an extraordinarily productive scientific facility time and time again, and we greatly appreciate the support of policymakers, and all those in the flight and servicing programs who contributed to the repeated successes of the *HST* servicing missions. P.O. acknowledges support from the Swiss National Foundation (SNF). This work has been supported by NASA grants NAG5-7697 and HST-GO-11563.01.

Facilities: HST (ACS/NICMOS/WFC3)

REFERENCES

Beckwith, S. V. W., et al. 2006, AJ, 132, 1729
Bouwens, R. J., et al. 2004, ApJ, 611, L1
Bouwens, R. J., et al. 2006, ApJ, 653, 53
Bouwens, R. J., et al. 2009a, ApJ, submitted (arXiv:0909.1803)
Bouwens, R. J., et al. 2009b, ApJ, 705, 936
Buitrago, F., et al. 2008, ApJ, 687, L61
Bunker, A. J., et al. 2009, MNRAS, in press (arXiv:0909.2255)
Conselice, Ch. J., & Arnold, J. 2009, MNRAS, 397, 208
Dekel, A., et al. 2009, ApJ, 703, 785
Ferguson, H. C., et al. 2004, ApJ, 600, 107
Finlator, K., et al. 2006, ApJ, 639, 672
Firmani, C., et al. 2009, MNRAS, 396, 1675
Giavalisco, M., et al. 1996, ApJ, 470, 189
Giavalisco, M., et al. 2004a, ApJ, 600, L93
Giavalisco, M., et al. 2004b, ApJ, 600, L103
Hathi, N. P., et al. 2008a, AJ, 135, 156
Hathi, N. P., et al. 2008b, ApJ, 673, 686
Law, D. R., et al. 2007, ApJ, 656, 1
Lotz, J., et al. 2006, ApJ, 636, 592
Lowenthal, J., et al. 1997, ApJ, 481, 673
Madau, P., et al. 1998, ApJ, 498, 106
McLure, R. J., et al. 2009, MNRAS, in press (arXiv:0909.2437)
Meurer, G. M., et al. 1997, AJ, 114, 54
Meurer, G. M., et al. 1999, ApJ, 521, 64
Mo, H. J., et al. 1998, MNRAS, 295, 319
Mo, H. J., et al. 1999, MNRAS, 304, 175
Nagamine, K., et al. 2008, arXiv0802.0228
Night, C., et al. 2006, MNRAS, 366, 705
Oesch, P. A., et al. 2007, ApJ, 671, 1212
Oesch, P. A., et al. 2010, ApJL, 709, L16
Oke, J. B., & Gunn, J. E. 1983, ApJ, 266, 713
Overzier, R. A., et al. 2008, ApJ, 677, 37
Peng, C. Y., et al. 2002, AJ, 124, 266
Petty, S. M., et al. 2009, AJ, 138, 362
Ravindranath, S., et al. 2006, ApJ, 652, 963
Somerville, R. S., et al. 2001, MNRAS, 320, 504
Somerville, R. S., et al. 2008, ApJ, 672, 776
Steidel, C., et al. 1996, ApJ, 462, L17
Steidel, C., et al. 1999, ApJ, 519, 1
Walter, F., et al. 2009, Nature, 457, 699